6He breakup dynamic polarization potential reexamined

R. S. Mackintosh*

Department of Physics and Astronomy, The Open University, Milton Keynes, MK7 6AA, United Kingdom

N. Keeley†

Department of Nuclear Reactions, The Andrzej Sołtan Institute for Nuclear Studies, Hoża 69, PL-00681 Warsaw, Poland

The dynamic polarization potential contribution to the effective interaction between 6He and 208Pb at 27 MeV, due to breakup channels, is recalculated exploiting a recently developed improved model for 6He. The most general features of the long-range attractive and absorptive components remain the same as were found in an earlier study, but the asymptotic magnitudes are reduced by factors of about 2.5 and 4.5, respectively. We draw conclusions from these results, as well as from further calculations at 22 MeV, closer to the Coulomb barrier, and at 32 MeV.

I. INTRODUCTION

The scattering of the halo nucleus 6He from the high-Z nucleus 208Pb is strongly influenced by the coupling to breakup states in the continuum. This is reflected in the properties of the dynamical polarization potential (DPP) generated by this coupling. In particular, the dipole excitation leads to DPPs having exceptionally long-ranged real and imaginary components, as explicitly presented in Refs. [1–3]. The main purpose of this work is to present revised DPPs, taking advantage of a greatly improved cluster model [4] for 6He. The nature of this new model is such that we expect considerable modifications to the DPP. In the process of considering the new complex DPP and its relation to the old, a number of significant features have emerged that we also describe.

Our general procedure is as before: the elastic scattering of 6He is calculated with account taken of the coupling to states in the continuum using the continuum discretized coupled-channels (CDCC) method [5] implemented in the code FRESCO [6]. The elastic scattering S-matrix S_L from the CDCC calculations is then subject to $S_L \rightarrow V(r)$ inversion using the iterative-perturbative (IP) method described in Ref. [7]. A measure of the quality of the inversion is the "inversion distance" $\sigma_{\rm inv}$, defined, in the context of IP inversion for spinless particles, from the expression for its square:

$$\sigma_{\rm inv}^2 = \sum_L \left| S_L^{\rm tar} - S_L^{\rm inv} \right|^2, \tag{1}$$

where $S_L^{\rm tar}$ is the ("target") S matrix that is to be inverted and $S_L^{\rm inv}$ is the S matrix for the inverted potential. It is often possible to achieve values of $\sigma_{\rm inv}$ corresponding to $S_L^{\rm tar}$ and $S_L^{\rm inv}$ that are indistinguishable on a graph, although the actual values of $\sigma_{\rm inv}$ will depend on context such as the projectile spin, the number of partial waves, and the "noisiness" of the input $S_L^{\rm tar}$.

The complex local potential found by inversion, $V_C(r)$, having small $\sigma_{\rm inv}$, would, if inserted into an optical model

(single channel) code, very closely reproduce the theoretical elastic scattering from the CDCC calculations. Subtracting the complex bare potential employed in the CDCC calculations, $V_B(r)$, then yields a local and L-independent representation of the DPP, $V_D(r) = V_C(r) - V_B(r)$,

Initially, the calculations were carried out at 27 MeV, as in Ref. [1] and in Moro *et al.* [4]. To explore the breakup DPP at an energy region closer to the barrier, we also calculated the DPP at 22 MeV. Finally, calculations at 32 MeV were also carried out to settle certain questions arising from the 22- and 27-MeV calculations. The results of calculations at several energies would, in principle, provide the means for a comparison with the properties of the long-range DPP that would result from the semiclassical Coulomb dipole model of Andrés *et al.* [8].

II. CALCULATION OF THE DPP

A. The model of Moro *et al.*

Moro *et al.* [4] developed a two-body $2n$-α cluster model (hereafter, Moro-model) of 6He specifically for application to the scattering of this nucleus from high-Z nuclei such as 208Pb. The parameters of the two-body model were chosen to reproduce relevant properties of a three-body model. The Moro-model reproduces not only the distribution of dipole strength suggested by a three-body model but also the $B(E2)$ transition strength, including the sharp 2^+ resonance at 1.8 MeV. Moro *et al.* demonstrate that their model reproduces low-energy 6He elastic-scattering data.

The present updating of our calculations is particularly necessitated by two significant properties by which the Moro-model differs from that used previously in Refs. [1,2]. These are as follows: (i) the low-energy dipole coupling strength $B(E1)$ to the continuum is considerably smaller and (ii) the spatial extension of the ground state is significantly smaller. We shall indicate the specific features of the complex DPP that are influenced by these properties.

---

*r.mackintosh@open.ac.uk
†keeley@fuw.edu.pl

B. The CDCC calculations

The CDCC calculations presented here for 27 MeV repeat exactly those of Moro *et al.* [4] for ^{6}He + ^{208}Pb. The same $2n + \alpha$ binding potentials and $2n + ^{208}$Pb and $\alpha + ^{208}$Pb optical potentials were employed, along with an identical binning scheme for the $2n + \alpha$ continuum of ^{6}He. All interchannel couplings are included, except as specifically noted in certain cases.

For the calculations at 22 and 32 MeV we used the same $2n + ^{208}$Pb and $\alpha + ^{208}$Pb optical potentials as at 27 MeV to ensure that any energy dependence of the DPP that we observe is purely dynamical in origin. Although the global deuteron potential used as a surrogate for the $2n + ^{208}$Pb optical potential does have energy-dependent real and imaginary well depths, ignoring this dependence leads to physically reasonable results in this case. As evidence of this, the full CDCC calculation gives a good description of the 22 MeV ^{6}He + ^{208}Pb elastic-scattering data [9]. To study the specific contribution of the 2^+ resonance at 1.8 MeV, we also performed CDCC calculations that include only the coupling to this state.

III. PROPERTIES OF THE DPP AT 27 MeV

We first compare the CDCC elastic scattering S matrices with those calculated directly from the bare potential. In Fig. 1
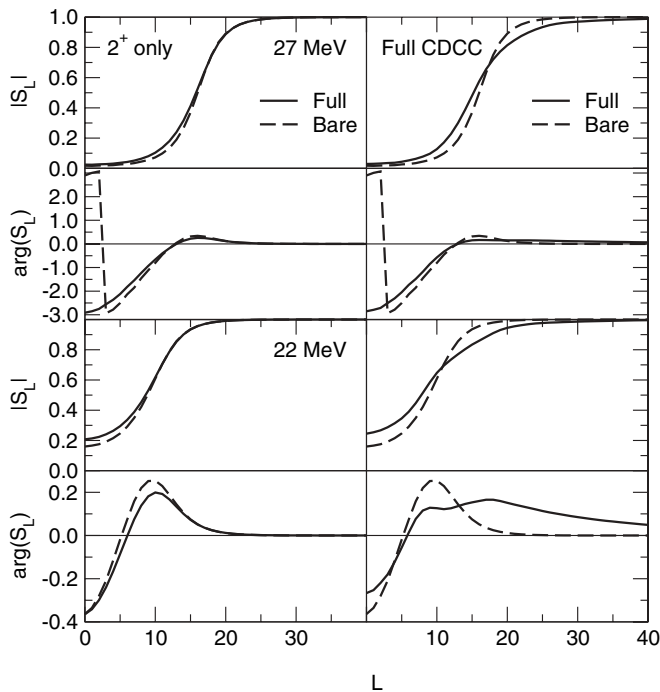

FIG. 1. The effect of coupling on the elastic-scattering S matrix. On the left we show the effect of just the 2^+ resonance, and on the right, of the full set of continuum states. In all cases, the solid line represents the S matrix with the coupling included, and the dashed line the S matrix calculated from the bare potential. The top half of the figure presents the 27-MeV results and the bottom half the 22-MeV results. Finally, in each section, $|S_L|$ is given above and $\arg(S_L)$ below, with a different scale at 22 MeV.

we present $\arg(S_L)$ and $|S_L|$, quantities that, for weakly absorbed projectiles at least, are predominantly related to the real and imaginary parts of the potential, respectively (see appendix of Ref. [10]). The left-hand panels of Fig. 1 refer to CDCC calculations in which only the 2^+ resonance is excited and the right-hand side refers to the full calculations. The upper half of the figure presents S_L at 27 MeV and the lower half at 22 MeV. Within each of these four sections, $|S_L|$ is in the upper panel and $\arg(S_L)$ in the lower. Note that $\arg(S_L)$ is plotted on a different scale at 22 MeV, reflecting the smaller penetration at the lower energy. In each case, S_L for the full CDCC calculation is shown with a solid line and S_L for the bare potential with a dashed line. Examining $|S_L|$ on the left, we see that coupling to the 2^+ resonance has little effect for $L > 10$ at 22 MeV apart from a very slight decrease, just visible, around $L = 14$. There is a corresponding decrease for 27 MeV around $L = 20$ but less than the thickness of the lines in the figure. The conspicuous effect in each case is for coupling to the 2^+ state to generate a notable *increase* in $|S_L|$ for low L, with the larger effect at 22 MeV, closer to the barrier. In general, such an increase is expected with a reduced absorption of flux. Such an increase over limited ranges of L, induced by channel coupling, frequently occurs and is sometimes attributed to nonlocal effects. A full understanding of how DPPs are generated by coupling requires an account of such counterintuitive features.

The effect of coupling to the 2^+ resonance on $\arg(S_L)$ is also confined to low L at both energies. However, referring to the right-hand side of the figure, the effect of the full coupling extends to very high L, far off the graph. At both energies the increase in $|S_L|$ for low L is slightly greater than it was with just 2^+ coupling, but, for higher L, $|S_L|$ shows the expected significant reduction and $\arg(S_L)$ is significantly increased. These effects are directly related, respectively, to absorption and attraction at large radii. The attractive effect remains substantial out to a larger value of L than the absorptive effect, and we expect a corresponding greater radial extent for the real DPP. We note in particular: (i) the effect on S_L is notably greater at 22 MeV than at 27 MeV though qualitatively similar and (ii) much but not all of the effect for lower L is due to quadrupole coupling to the 2^+ state.

The DPPs corresponding to the S matrices for the full Moro-model calculation at 27 MeV are presented in Fig. 2 where they are compared with the those calculated using the old model [1] for ^{6}He. The very-long-range attraction and absorption are apparent in the lower panels. The real part is, as it was for the old calculation, greater in magnitude than the imaginary and extends further out. Although the overall magnitudes of the real and imaginary parts are substantially reduced with the Moro-model, the relative relationships are enhanced: the asymptotic strength of the real part is reduced by roughly a factor of 1/2.5 whereas that of the imaginary part is reduced by 1/4.5. This specific result merits comparison with the semiclassical Coulomb dipole model of Ref. [8] according to which the asymptotic DPP depends only on $B(E1)$ strength and kinematic factors.

The characteristic effect of Coulomb dipole excitation is often described as *long-range absorption,* and indeed this is what is suggested by optical model analyses. Nevertheless,
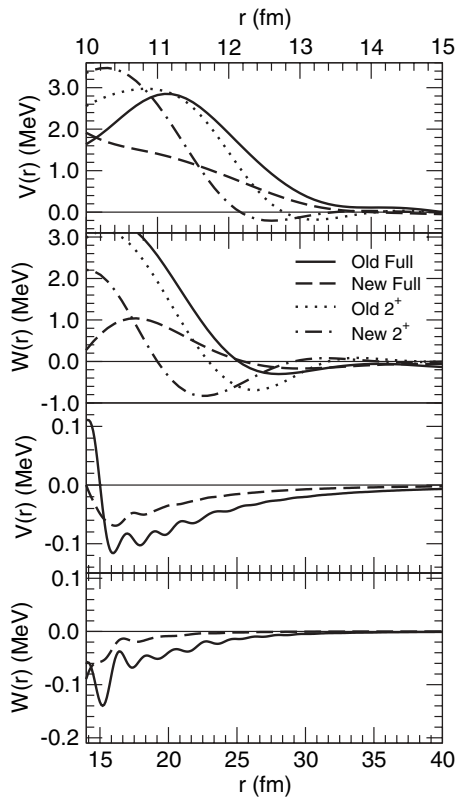
FIG. 2. The DPP generated by coupling to the new (Moro) full set of continuum states at 27 MeV (dashed lines) compared with the "old" DPP of Ref. [1] (solid lines). The top two panels show the inner radial range, 10 to 15 fm, with the radial scale given at the top. The outer radial range, from 14 to 40 fm, is shown in the lower two panels. The upper two panels also show the DPP arising from the coupling to the 2^+ state, dotted for the "old" model, and dot-dashed for the Moro model. DPPs due to the 2^+ state are negligible in the outer region.

this is not what is suggested by the relative strengths of the real and imaginary parts of the asymptotic DPPs shown in Fig. 2. Instead, it would appear that the characteristic effect of Coulomb dipole breakup coupling is more *long-range attraction* than long-range absorption, as also found in Ref. [3]. The title itself of this last reference ("Long range absorption...") emphasizes the phenomenologically significant aspect. The apparent contradiction between the properties of the derived DPP and the findings of phenomenology is specifically addressed in Sec. VI.

The upper panels of Fig. 2 also show the DPP for smaller r: the effect is repulsive and emissive around 11 fm. The emissive region of the DPP is probably related to the increase in $|S_L|$ for lowest L. The underlying DPP, represented here by its local equivalent, is nonlocal, and the somewhat counterintuitive emissive region of the local DPP, arising from channel coupling, may be a consequence of this; this degree of emissiveness will not, of course, lead to unitarity breaking. The real part of the DPP for smaller r corresponds to roughly 2 MeV of repulsion near the Coulomb barrier. Both the real and imaginary Moro-model DPPs differ from the old in being shifted to somewhat smaller radii, an effect naturally attributed to the smaller spatial extension of the Moro-model
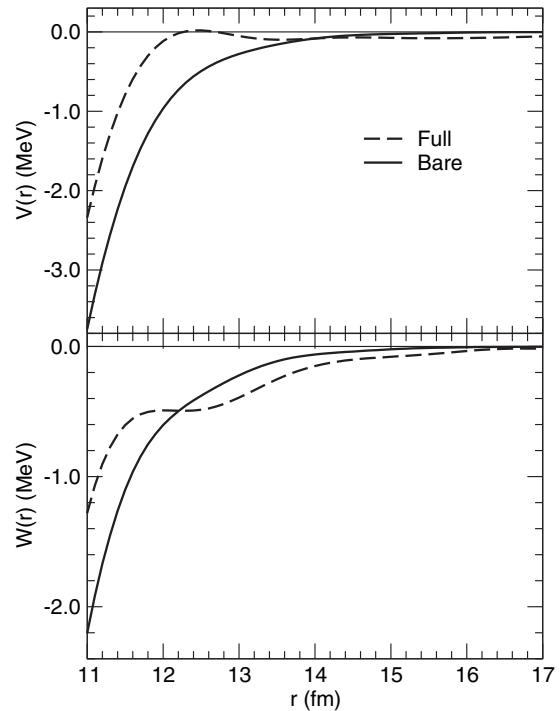

FIG. 3. Comparing the bare potential (solid lines) with the potential generated by inverting the CDCC Moro model S matrix at 27 MeV (dashed lines). The real part is in the top panel with the imaginary part below, with a different vertical scale.

wave function. The DPPs are plotted down to a radius of 10 fm; notch tests (see Sec. V) indicate considerable sensitivity down to 10 fm, a radius that is much less than the strong absorption radius, SAR. Using the CDCC S matrix and the criterion $|S_L| = \frac{1}{2}$, we find the SAR to be 11.7 fm.

It is general properties rather than precise point-by-point values that are well-determined by inversion for $r > 10$ fm and below $r \sim 11.5$ fm, the ^{6}He nucleus being strongly absorbed. Plots of the DPPs alone do not reveal their substantial contribution to the potential and Fig. 3 compares, over the surface region, the bare potential and the potential that was inverted from the full CDCC S matrix at 27 MeV. It can be seen that the imaginary potential is nowhere actually emissive, although considerably reduced around 11.5 fm, but the real potential does just become repulsive near 12.5 fm. This figure makes it clear that the effects of channel coupling are not well represented by renormalizing a folding model potential; unfortunately, this may be hard to discern in cases where the elastic-scattering data determines the potential only over a narrow radial range.

The upper panels of Fig. 2 also present the DPPs that arise from the calculations when only the coupling to the 2^+ resonance is included. These DPPs are negligible for $r > 15$ fm, consistent with the behavior of S_L in Fig. 1. The repulsive effect in the inner region is similar to that found for the full calculations, with the DPPs arising from the Moro-model excitation again shifted to smaller radii compared with the DPPs from the older model. The DPPs shown in this figure imply that the 2^+ resonance makes a major contribution to the full DPP over the inner radial range. However, the

interchannel coupling between the 2^+ resonance and the other continuum states makes the correspondence less clear-cut.

IV. ENERGY DEPENDENCE OF THE DPP

It is of interest to examine the DPP closer to the Coulomb barrier and for this reason we repeated the Moro-model calculations, with full continuum couplings, at 22 MeV, an energy for which there are elastic-scattering data [9]. To establish whether the resulting energy dependence continued to higher energies, we also established the DPPs at 32 MeV. Figures 4, 5, and 6 compare the resulting DPPs at all three energies over three overlapping radial ranges, with different scales. The short-range DPPs, Fig. 4, appear to have little energy dependence. However, although the long-range attractive and absorptive DPPs have the same general form, the asymptotic DPPs are energy dependent, Fig. 6, with the real part increasing slightly with energy and the imaginary part increasing substantially with energy. These long-range DPPs are the result of Coulomb dipole excitation, and it would be interesting and meaningful to compare the relative strengths, asymptotic forms and energy dependencies of the real and imaginary parts with the same properties derived from the semiclassical theory of Ref. [8].

Figure 7 shows the energy dependence of the DPP that results from coupling to the 2^+ state alone. A consistent pattern is revealed although the emissive region at $r \sim 11$ fm in the 22-MeV case cannot be regarded as well established; the
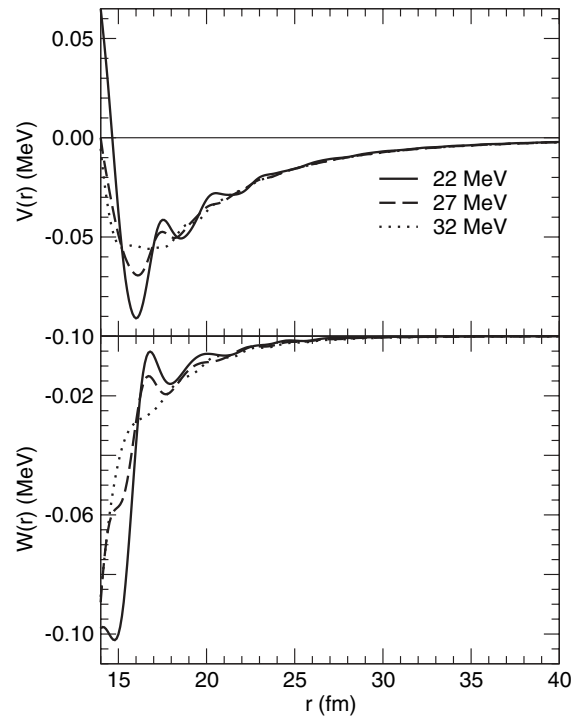

FIG. 5. The DPP generated by coupling to the full set of continuum states for the Moro-model at 22 MeV (solid lines), 27 MeV (dashed lines), and 32 MeV (dots). The DPPs are presented between 14 and 40 fm. The real part is in the top panel with the imaginary part below.
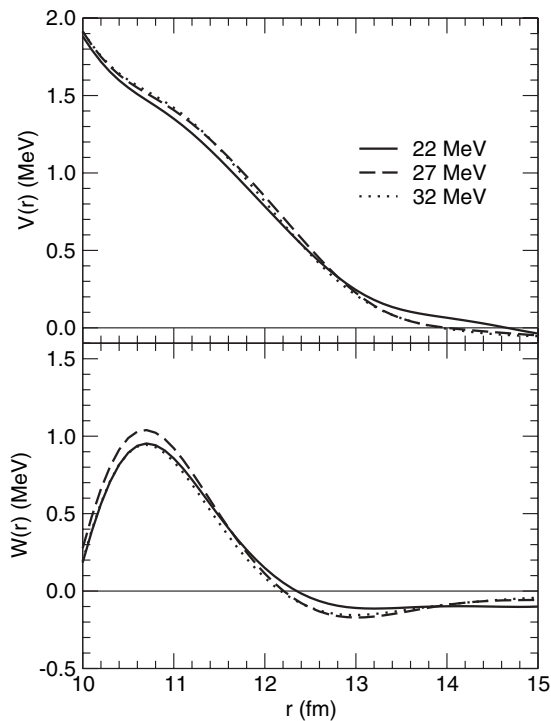

FIG. 4. The DPP generated by coupling to the full set of continuum states for the Moro-model at 22 MeV (solid lines), 27 MeV (dashed lines), and 32 MeV (dots). The DPPs are presented between 10 and 15 fm. The real part is in the top panel with the imaginary part below.
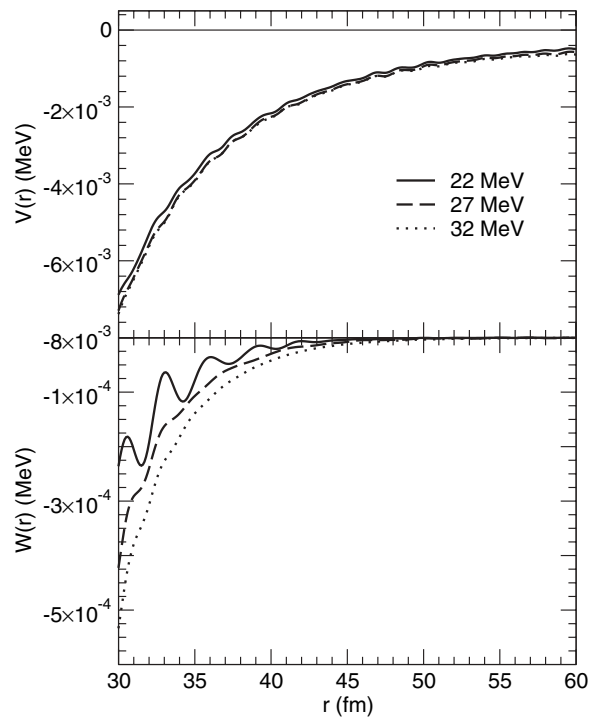

FIG. 6. The DPP generated by coupling to the full set of continuum states for the Moro-model at 22 MeV (solid lines), 27 MeV (dashed lines), and 32 MeV (dots). The DPPs are presented between 30 and 60 fm. The real part is in the top panel with the imaginary part below.
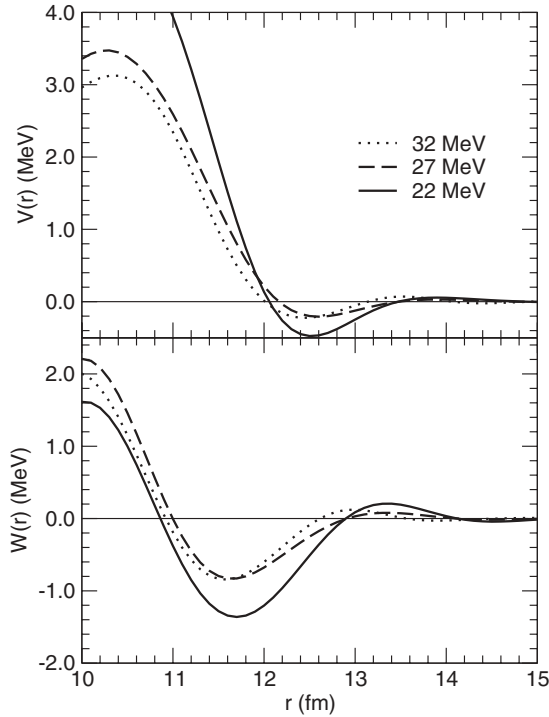
FIG. 7. The DPP generated by coupling to 2^+ resonance for the Moro-model at 22 MeV (solid lines), 27 MeV (dashed lines), and 32 MeV (dots). The real part is in the top panel with the imaginary part below.

inverted potential at 22 MeV is not well defined in this radial region, a consequence of the greater absorption at the lower energy.

In view of the considerable difference between S_L at 22 and 27 MeV, apparent in Fig. 1, it is interesting that the difference between the DPPs at these two energies is quite small.

V. NOTCH TESTS

For ⁶He nuclei interacting with ²⁰⁸Pb at the energies considered here, the potential returned by the IP inversion procedure becomes ill determined in the region where the two nuclei strongly overlap, and for that reason we have not presented potentials for $r < 10$ fm. We have studied sensitivity of the 27-MeV inverted potential, over the radial range between 9 and 11 fm, by adding a Gaussian notch

$$V(r) = V_0 \exp[-((r - R)/a)^2] \quad (2)$$

with varied R and $a = 0.3$ fm to the real and alternatively to the imaginary inverted potentials. As R varied, we noted the consequent change in σ_{inv}, defined in Sec. I. V_0 was chosen to be $0.05 \times$ the real part of the bare potential at R. The notch (attractive or absorptive in sign) is small compared to the potential that is being tested (bare plus DPP) in the region of the SAR. Generally, notch tests monitor changes in χ^2/N but there are insufficient data at 27 MeV to make that meaningful here.

The results can be briefly summarized (a more detailed account is in preparation [11]) as follows:

(i) σ_{inv} is increased by a factor of 3 for either a real or imaginary notch at $r = 10$ fm.

(ii) the pattern of increase in σ_{inv} as R varies, and the corresponding pattern of change in the reaction cross section are both remarkably independent of whether the notch is in the real or imaginary potential.

(iii) In spite of point (ii), the effects of real and imaginary notches on the angular distributions are quite different from each other. In particular, an imaginary notch at 11 fm affects σ_{inv} markedly but has little effect on the differential cross section, whereas a real notch at the same radius may have an almost identical effect on σ_{inv} but does have a marked effect on the differential cross section. Optical model fitting of precise data should in principle determine the real potential at the radius in question.

(iv) Point (iii) is related to the fact that a real notch at 11 fm modifies $|S_L|$ and an imaginary notch modifies just $\arg(S_L)$. This is precisely the opposite of what is found for weakly absorbed projectiles [10].

Point (i) answers the question that was the initial motivation for carrying out the notch tests: the potential is, in a sense, defined by the notch test, significant down to 10 fm. It is for that reason that we have plotted the potentials from that radius. However, we note that the inversion probably does not yield a point-by-point unique potential down to that radius although the general character does appear to be well established.

Point (iii) may well explain the observation on page 41 of Ref. [9], relating to ⁶He on ²⁰⁸Pb at energies around the Coulomb barrier, that the radial range of sensitivity lies much further within the overlap region for the real part than it does for the imaginary part.

The other three points seem to raise interesting questions for phenomenology and questions concerning the meaningfulness of potentials. In particular, there may be situations where there are radial regions where a potential cannot be reliably established by conventional fitting methods but over which the potential is nevertheless a meaningful concept and could be relevant to nonelastic processes.

VI. LONG-RANGE ATTRACTION OR ABSORPTION?

Coulomb dipole excitation is commonly referred to as resulting in long-range absorption whereas, as shown here and also in Ref. [3], the real part of the external DPP is both greater in magnitude and longer in range than the imaginary part. It is *not* simply a result of the bare potential being larger in the surface, so the effect of changes in the real part seems smaller relative to this. To understand the relative contribution of the real and imaginary tails, we examined the effect of cutting off the real or imaginary tail by multiplying the inverted potential with the factor

$$f(r) = \frac{1}{1 + \exp[(r - R)/a]}. \quad (3)$$

where we chose $R = 14$ fm and $a = 0.5$ fm (notch tests are not helpful for large r). We found that the effects of truncating the real tail, on both the differential cross section and the total reaction cross section, are much less than the effects of truncating the imaginary tail. This is in spite of the greater magnitude of the real tail. In contrast, there is a much *greater* effect of truncating the real potential on the inversion distance σ_{inv} than there is of truncating the imaginary potential. The most probable resolution of this seemingly paradoxical behavior is a conjunction of two facts:

(i) truncating the real potential tail modifies $\arg(S_L)$ while having almost no effect on $|S_L|$, while truncating the imaginary tail affects just $|S_L|$. This is behavior that is typical of weak absorption and is in accord with Ref. [10] but is in complete contrast to what was found in point (iv) of Sec. V concerning a notch at 11 fm.

(ii) the almost complete nearside dominance of scattering in this case. As a result, although cutting the real potential tail greatly modifies the phase of S_L for large L, there is no opportunity for this to result in interference between contributing amplitudes.

The calculations with truncated potentials also revealed the importance of the inner region of the DPP, i.e., for $r < 14$ fm. Specifically, the imaginary tail for $r > 14$ fm turns out to be responsible for some, but not all, of the reduction of the differential cross section at the rainbow peak. Such a peak is evident with the bare potential. The real part of the tail has very little effect on this, and we conclude that the DPP for $r < 14$ fm, the imaginary part in particular, contributes to the absence of a rainbow peak in the angular distribution.

All these general results of truncating the real and imaginary tails apply at all three energies.

VII. CONCLUSIONS

As expected, the ^{6}He wave functions of Moro *et al.* [4] resulted in a considerably reduced long-range DPP compared to the wave function employed in Refs. [1,2]. This is the immediate result of the lower value of $B(E1)$. What is less obvious is that the lower $B(E1)$ leads to a significantly different ratio of real to imaginary long range DPP and a different falloff with r. We also found that the DPP in the range of 10 to 14 fm, which makes a significant contribution to the shape of the differential cross section, was shifted inward. This presumably corresponds to the reduced radial extent of the Moro-model wave function and suggests why the Moro model gives a better description of the scattering in the region of the Coulomb rainbow.

The long-range tail of the DPP is due to Coulomb dipole excitation and governed in semiclassical models [8] just by $B(E1)$ and kinematics. The particular changes in strength and extension of the real and imaginary tails found here merit future comparison with the predictions of such models.

In the course of evaluating these results, a number of somewhat counterintuitive effects emerged. For example, in the nuclear interior (but not in the surface) changes to the *real* potential modify $|S_L|$, whereas changes to the *imaginary* potential affect $\arg(S_L)$. This reversal of the expected might be related to the fact, also found here but previously known, that strongly coupled channels can *increase* $|S_L|$ over specific ranges of L. This is presumably related to the underlying nonlocality of the DPP, represented here as a local potential. It appears that much still remains to be understood concerning nucleus-nucleus scattering and the meaning of potential models. In connection with the last point, we plan to study the difference between the potentials that fit the inverted S_L, the TELP potentials extracted from the CDCC wave function [6], and the potentials that fit the data [3].

[1] R. S. Mackintosh and N. Keeley, Phys. Rev. C **70**, 024604 (2005).

[2] N. Keeley and R. S. Mackintosh, Phys. Rev. C **71**, 057601 (2005).

[3] O. R. Kakuee, M. A. G. Alvarez, M. V. Andres, S. Cherubini, T. Davinson, A. Di Pietro, W. Galster, J. Gómez-Camacho, A. M Laird, M. Lamehi-Rachti, I. Martel, A. M. Moro, J. Rahighi, A. M. Sánchez-Benitez, A. C. Shotter, W. B. Smith, J. Vervier, and P. J. Woods, Nucl. Phys. **A765**, 294 (2006).

[4] A. M. Moro, K. Rusek, J. M. Arias, J. Gómez-Camacho, and M. Rodríguez-Gallardo, Phys. Rev. C **75**, 064607 (2007).

[5] G. H. Rawitscher, Phys. Rev. C **9**, 2210 (1974); Y. Sakuragi, M. Yahiro, and M. Kamimura, Prog. Theor. Phys. Suppl. **89**, 136 (1986).

[6] I. J. Thompson, Comput. Phys. Rep. **7**, 167 (1988).

[7] V. I. Kukulin and R. S. Mackintosh, J. Phys. G: Nucl. Part. Phys. **30**, R1 (2004).

[8] M. V. Andrés, J. Gómez-Camacho, and M. A. Nagarajan, Nucl. Phys. **A579**, 273 (1994).

[9] A. M. Sánchez-Benítez, D. Escrig, M. A. G. Álvarez, M. V. Andrés, C. Angulo, M. J. G. Borge, J. Cabrera, S. Cherubini, P. Demaret, J. M. Espino, P. Figuera, M. Freer, J. E. García-Ramos, J. Gómez-Camacho, M. Gulino, O. R. Kakuee, I. Martel, C. Metelko, A. M. Moro, F. Pérez-Bernal, J. Rahighi, K. Rusek, D. Smirnov, O. Tengblad, P. Van Duppen, and V. Ziman, Nucl. Phys. **A803**, 30 (2008).

[10] R. S. Mackintosh and A. M. Kobos, J. Phys. G: Nucl. Part. Phys. **5**, 359 (1979).

[11] N. Keeley and R. Mackintosh (manuscript in preparation).